

New Hypercoordinating Organostannanes for the Modular Functionalization of Mono- and Polystannanes: Synthetic and Computational Studies

Jeffrey Pau,^a Jung-Won Choi,^a Kaitlyn Silverthorne^a, Mokhamed Ranne^a, R. Stephen Wylie^a, Robert A. Gossage^a, Alan J. Lough^b and Daniel A. Foucher^{*a}

A series of potentially hypercoordinate tin compounds derived from a substitutionally labile stannane was produced to gain access to a library of stannanes and polystannanes for structure/property investigations. Three model triphenylstannanes, containing either a propyloxybiphenyl (**11**), propylmethoxy (**12**) or propylthioester (**13**) group were synthesized in high yields via substitution reactions of the propyl tosylated stannane **4**. Compounds **12** and **13** were converted to the appropriate mono-(**14**, **15**) and dichlorido-(**18**, **19**) stannanes via sequential chlorinations with HCl. Further transformation of **18** or **19** to the dihydrido (**22**, **23**) was carried out with the use of an appropriate reducing agent. Structural characterizations by single crystal X-ray diffraction of **12**, **14**, **18** and **19** were also undertaken and are discussed. Several DFT methods were compared for accuracy in predicting the hypercoordinate geometries of these compounds. The relative energies of hypercoordinate conformers for the propylmethoxystannanes **12**, **14**, **18**, and **22** were determined and the fractional abundance of each conformer in the gas and solution (CHCl₃) phase was estimated. Relativistic DFT calculations of ¹¹⁹Sn NMR chemical shifts were carried out for a series of non-hypercoordinate reference compounds and the conformers, allowing the estimation of Boltzmann-averaged chemical shifts of the propylmethoxystannanes. A semi-crystalline homopolymer (**25**) was isolated from the dehydropolymerization of **22** using Wilkinson's catalyst. Conversion of the labile tosylated polystannane (**24**) to a new partially substituted polystannane (**28**) via nucleophile displacement reactions was achieved. The structures of model stannanes, chlorinated stannanes, hydrido stannanes and polystannanes were confirmed via NMR (¹H, ¹³C, ¹¹⁹Sn) spectroscopy, HRMS, and, in the case of the polymers (**25**, **28**), also by elemental analysis, GPC, DSC and PXRD (**25**).

^a Department of Chemistry and Biology, Ryerson University, 350 Victoria Street, Toronto, Ontario, Canada M5B 2K3, E-mail: daniel.foucher@ryerson.ca

^b Department of Chemistry, X-Ray Laboratory, University of Toronto, Toronto, ON, Canada M5H 3H6, E-mail: alough@chem.utoronto.ca

Introduction

Polystannanes are main group polymers with a conjugated backbone of tin atoms prepared from the reductive coupling of dihalido- or dihydrido- diorganostannane monomers.^{1,2} Sodium (Wurtz)³⁻⁵ or electrochemical coupling^{6,7} of X₂SnRR' leads directly to the desired materials, while conversion of such materials to diorganostannanes, H₂SnRR' followed by transition metal catalyzed dehydropolymerization⁸⁻¹⁰ affords the target polystannanes. Key to both approaches is access to both homo- and hetero-diorganostannanes. This is traditionally achieved by the Kocheshkov reaction, a solventless redistribution of organo and halogen substituents at tetracoordinated tin centers to afford the required organohalo (R_{4-n}SnCl_n) tin species.¹ Experimentally, alkyl substituents have been more difficult to selectively interchange than aryl ones (*n*-Bu < Me < Ph < Mes).¹ Interestingly, an increase of coordination number at tin from four to six has a notable impact on these redistribution reactions. Utilizing van Koten's N,C,N pincer ligand,¹¹ (2,6-(Me₂NCH₂)C₆H₃)-, Růžička and coworkers reported a partial redistribution at RT of an intramolecularly bound monochlorostannane (Figure 1, **1**) in solvent to the dichlorostannane and the triphenylstannane after a 2 week time period.¹² Nechaev and co-workers later detailed the high yield redistribution reaction of six coordinate PhSn(κ²-O, N-OCH₂CH₂NMe₂)₂Cl (Figure 1, **2**) with PhSnCl₃ to the symmetrical dialkoxydichlorostannane and Ph₂SnCl₂ species.¹³ In both examples, the presence of hypercoordinating interactions from the tethered donor side chains lead to a "reversed" redistribution of these organotin compounds.

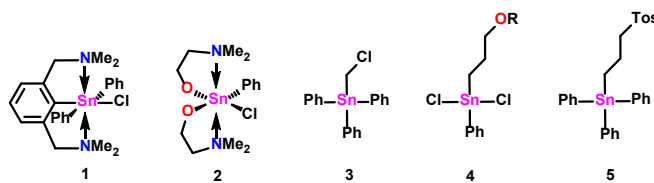


Figure 1: Schematic representations of compounds 1-5 (R = aryl, Tos = tosylated).

Functionalization of stannanes from chlorido or hydrido triorganostannanes has been demonstrated by the teams of Pace and Molloy, respectively. Tandem homocoupling of triorganohalostannanes with modified methyl lithium reagents (e.g. LiCH_2Cl) yielded α -functionalized monohalomethyl stannanes (**3**) in good yields (> 80%).¹⁴ Molloy reported the preparation of dihalodiodiorganostannanes **4** (Figure 1) from an initial hydrostannylation of triphenylstannane with an allyl ether or allyl alcohol substituents, followed by stoichiometric bromination.⁴ Our research¹⁵ has demonstrated displacement reactions of the tosyl substituent in **5** (Figure 1) with 4-hydroxyazobenzene under Williamson ether-like conditions. This approach may be an effective general method to prepare a variety of hypercoordinating stannane monomers for moisture and light stable polystannanes.

Access to a wide variety of functional organic polymers from a single sacrificial macromolecular intermediate has been a successful strategy for the last three decades.¹⁶ Post-polymerization modification of an intermediate using comparatively mild transformations enables the preparation of polymers that are otherwise hard to access, or sensitive to the polymerization conditions. Additionally, new polymers derived from a single, high yielding, low-cost macromolecular intermediate provides an opportunity to probe structure-property relationships between materials built from a common modular structural platform.

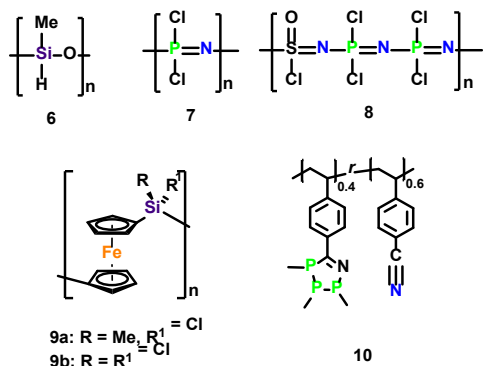


Figure 2: Select inorganic and organometallic polymers.

Post-polymerization of main group and organometallic polymers is relatively unexplored with a few notable exceptions. Modification of poly(methylhydrosiloxanes), **6** (Figure 2), with vinylsiloxanes via transition metal-catalyzed hydrosilylation¹⁷ and the nucleophilic substitution of the halo substituents of thermally ring-opened hexachloropolyphosphazene¹⁸ (**7**) or the closely related polythionylphosphazene (**8**) with alkoxy, amino or organo substituents has been established.¹⁹ In the mid 1990's, Manners and coworkers also demonstrated the tunable nature of thermally or transition metal-catalyzed ring-opened chlorinated sila[1]ferrocenophanes (**9a, b**) and were able to prepare substituted poly(ferrocenylsilanes) with sp , sp^2 and sp^3 moieties.²⁰ In 2017, this same group was able to demonstrate an "inorganic click" reaction with the cycloaddition of cyclophosphines to a polymeric styrene nitrile to yield **10**.²¹ This approach provides access to a host of tailored polymers bearing inorganic moieties. To gain access to a broader selection of hypercoordinated stannanes and polystannanes, we have carried out a three-part study. First, we have investigated the substitution chemistry of a model tosylstannane with three nucleophiles, preparing a library of small molecules using reactions potentially extensible to post-polymerization modifications. Second, we have estimated the extent of hypercoordination in solution for a subset of these small molecules using DFT calculations of geometries and ¹¹⁹Sn NMR chemical shifts, with comparison to experimental values. Finally, we disclose our first efforts to prepare tunable hypercoordinated polystannanes by post-polymerization modification of a previously known tosyl-containing polystannane.¹⁷ Functionally similar polymeric materials were also prepared by dehydrocoupling, where appropriate, for comparison.

Results and Discussion

Preparation of Model Stannanes

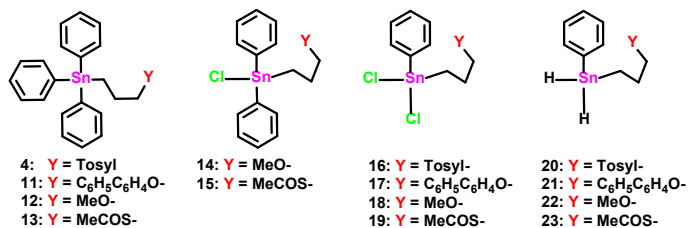
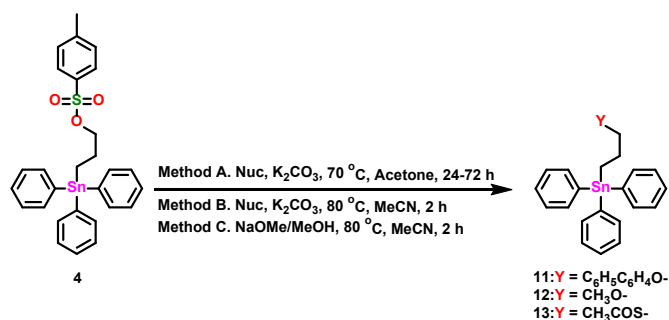


Figure 3: Organostannanes evaluated in this study.

The tosylstannane **4**,¹⁵ was prepared in two high yield steps following Yoshida's procedure without the need for column chromatography.²³ This air- and moisture-stable tosyl intermediate is also tolerant to acidic conditions, while substitutionally reactive under basic conditions. Conditions favourable for substitution at **4** (Figure 3) with the methoxy, thioacetyl and biphenyloxy nucleophiles were explored. Williamson ether and Williamson ether-like conditions (Scheme 1) in acetone (Method A) were initially used to prepare compounds **11** and **13** in low yields (< 40%) but was unsuccessful in the case of **12**. Higher yields of both **11** and **13** were obtained (> 75%) when the reaction was carried out in MeCN (Method B). High purity materials were isolated after extraction (without column chromatography) as determined by NMR spectroscopy (¹H, ¹³C, ¹¹⁹Sn), and for **11** was identical to material previously prepared by hydrostannylation protocols.⁴ Compound **13** was recovered as a yellow-coloured clear oil, in contrast to solid **11**.



Scheme 1: Reaction scheme for synthesis of model compounds **11-13**.

Compound **12** was readily prepared in good yield as a white coloured solid using NaOMe/MeOH in MeCN under mild conditions (< 2 h: Method C). As MeCN was also found to be preferable for substitutions of both the model stannanes and the tosyl polystannane, it was used exclusively thereafter. Compound **12** was recrystallized from DCM/hexanes and its solid-state structure established by X-ray crystallography (Figure 4: top left). This model triphenylstannane assumes a distorted tetrahedral geometry ($\tau_4 = 0.52$)²⁴ around the Sn centre. The Sn(1)-O(1) distance of **12** was 3.030(1) Å, falling within the van der Waals radii for Sn and O (3.69 Å) but exceeding typical Sn-O covalent bond lengths (2.05 Å).¹⁸

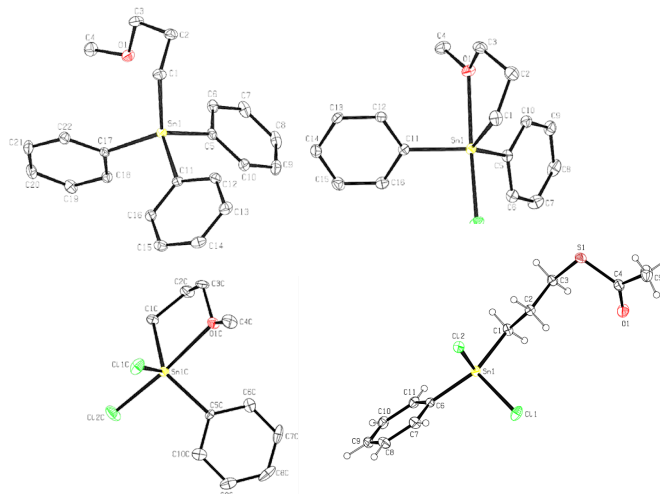
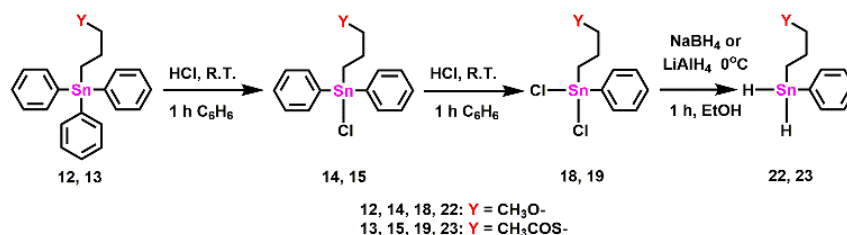


Figure 4: Displacement ellipsoid plots of **12** (top left), **14** (top right), one of the conformers of each **18** (bottom left) and **19** (bottom right). Thermal ellipsoids shown at the 30% level.

The new model stannanes **22** and **23** were prepared using established protocols.^{19,20} The three step process involved sequential chlorination of the model tristannanes (**12**, **13**) to monochlorides (**14**, **15**), then dichlorides (**18**, **19**) and finally, reduction to the dihydrido (**22**, **23**) compounds with a mild hydride source (Scheme 2).



Scheme 2: Preparation of functional stannanes used in this study.

Stannane **14** was obtained through an initial chlorination of **12** (>99% yield), with further conversion (>95%) to the dichlorinated stannane **18** after a second treatment with chlorinating reagent. Both crude chlorinated products were washed with a minimal volume of hexane, recrystallized from a solution of DCM and hexane and recovered as white crystalline solids. Similar transformations were achieved with compounds **15** and **19** in good yields and purity with isolation as a yellow-coloured semi-solid and orange-coloured crystals, respectively. The dihydridos (**22,23**) were isolated as white coloured semi-solids and kept at low temperature (-20 °C) and in the absence of light. Large upfield ¹¹⁹Sn NMR chemical shifts for these species were observed, consistent with a pseudo-tetrahedral, rather than trigonal bipyramidal geometry around tin. Further structural identification of the chlorinated methoxy-containing compounds **14** and **18** (Figure 4: top right, and bottom left respectively) by single crystal X-ray analysis reveals significant hypercoordination between the methoxy substituent and tin centres, similar to that observed previously by Lebl *et al.* for the closely related bis(3-methoxypropyl)tin dichloride species (Sn-O_{avg} 2.557 Å).²¹ Compound **14** presents approximate trigonal bipyramidal geometry (**14**: τ₅ = 0.90)²² and displays a short Sn-O bond distance (2.518(3) Å). The structure of **18** contains five independent molecules in the asymmetric unit, all structurally similar, with a geometry between trigonal pyramid and square pyramidal (**18**: τ₅ = 0.53_{avg}).²² The Sn-O distances are almost identical (averaging 2.445 ± 0.009 Å), in line with distances found in other closely related chlorinated stannanes.¹⁷ By contrast, the thioacetate-containing dichloride **19** (Figure 4, bottom right) reveals a fully extended propyl chain, with evidence of intermolecular hypercoordination. Two molecules of **19** form a dimer with paired Sn thioacetyl oxygen (Sn...O) separation distances of ≈ 2.88 Å. The dimers of **19** are weakly associated with other dimers through Sn...Cl intermolecular interactions of ≈ 3.36 Å, forming a pseudo-octahedral environment at the Sn centres. Similar propyl chain extension was reported previously in the structure of **16**.¹⁵

DFT Geometry Optimizations and Structural Comparisons

In two previous studies,^{23,24} we compared a total of 19 X-ray crystallographic structures of Sn hypercoordinate compounds with those calculated by a selection of computational DFT methods to assess which level of theory provided the best structural predictions. Although comparisons between experimental solid state and calculated gas phase structures are problematic for a variety of reasons,^{23,25,26} there are few other practical options.²⁷ In general, adding empirical dispersion to the computational methods significantly improved the accuracy of the calculated structures. The B3PW91²⁸ and PBE0 (“PBE1PBE”)²⁹ functionals supplemented with Grimme’s D3 empirical dispersion function and Becke-Johnson damping (GD3BJ)³⁰ were the best of ten methods studied;²³ the M052X³¹ method with Grimme’s D3 empirical dispersion (GD3) performed comparably.²⁴

In this study, nine crystallographic structures were compared using the three best DFT methods from the previous work as well as the MN15^{32,33} functional with GD3BJ empirical dispersion (see SI, Table S-1 for details). The four DFT methods used in geometry optimizations gave similar results, with the PBE0-GD3BJ method generally providing the best prediction of solid-state molecular geometries (Table S-1), as previously observed.^{23,24} The M05-2X method also performs well.

DFT Calculation of ¹¹⁹Sn NMR Chemical Shifts for Hypercoordinated Stannanes Conformers in Solution

Extending the computational modelling of these flexible stannane compounds to the calculation of solution-state properties presents three major challenges. First, due to the propyl linkages and hypercoordinate interactions, each of these compounds has several dozen stable conformations. Determining the ¹¹⁹Sn NMR chemical shift for a compound requires calculating the chemical shift for each geometrically optimized conformer, multiplying this by the conformer’s Boltzmann-weighted fractional contribution at the measurement temperature and then summing these. A second challenge is due to the solution state model. Implementation of a polarizable continuum model (PCM) for the solvent with quasi-ideal-gas statistical mechanics calculations of thermodynamic properties causes significant overestimation of translational and rotational entropies and thus systematic errors in Gibbs energy estimates.³⁴ Finally, it is not known which DFT functionals most accurately predict energies for these conformers in a PCM calculation.

In this study, we adopt some simplifying approximations to make the problem more tractable. First, we focus on the methoxystannane series **12**, **14**, **18**, and **22**, because these compounds only have one potentially hypercoordinating substituent (the methoxyl *O*-atom) and are the simplest structurally of the model stannanes in this study (Figure 3). Second, we assume that the most stable of the non-hypercoordinating conformers is the one with a fully extended propyl linker in an *anti*- methoxyl conformation. Third, the calculated solution state Gibbs energies are used for estimating Boltzmann averaged properties for a set of conformers for a given compound. Because the conformers are substantially similar, their translational and rotational entropies are nearly identical and the overestimation cancels out in the Boltzmann averaging. On that basis, we consider the accuracy of the relative Gibbs energies in the solution calculations to be comparable to the gas phase ones. Fourth, we use the PBE0-GD3BJ DFT method, given its good performance in predicting solid state geometries. Each of the compounds has multiple hypercoordinate conformers. For **14**, **18**, and **22**, the Sn substituent *trans*- to the hypercoordinating *O*-atom can vary (Ph and Cl or H) and there are also stable conformers with differing phenyl ring orientations. In hypercoordinate geometries, the methoxy- methyl can adopt an *anti*- or *gauche*- conformation with respect to C-2 of the propyl linkage. Only one *gauche*- conformer is observed because the other would bring the methyl group and Sn center into close proximity. The hypercoordinate and fully extended conformers for each of the methoxystannanes (**12**, **14**, **18**, and **22**) were determined by geometric optimization without and with solvation (chloroform) and verified with frequency calculations. As expected, hypercoordinate conformers are the lowest energy species, with *trans*-Cl stabilized relative to *trans*-Ph in **14** and **18** and *trans*-Ph stabilized relative to *trans*-H in **22**. The fractional abundance of each conformer for a given compound was estimated from the Gibbs energy differences. The amounts of the extended non-hypercoordinate conformers are negligible for **14** and **18**, and minor for **12** and **22**, suggesting that it is reasonable to ignore other higher energy non-hypercoordinate conformers. See SI and Table S-2 for details. The solvation model significantly alters the geometry of the hypercoordinate conformers, notably by reduction of the Sn-O distance (Table S-3). The most stable conformer remains the same for each of the compounds, but the relative energies and fractional abundances of the conformers change (Table S-2). The most stable hypercoordinate conformers for **12** and **22** are less stabilized relative to the extended conformers, while those of **14** and **18** are more so. Although the distribution of fractional abundances for the various conformers is similar with or without solvation, the differences are significant enough to influence the calculation of the ¹¹⁹Sn NMR chemical shifts.

DFT ^{119}Sn Chemical Shift calculations

The calculation of ^{119}Sn relative chemical shifts by DFT methods has been extensively studied³⁵ (for selected examples see Ref. ³⁶⁻⁴²). Non-relativistic calculations using the Gauge-Including Atomic Orbitals (GAIO) method and the all-electron IGLO II/III basis set are accurate for Sn compounds lacking other heavy atoms.^{36,38-40} Unfortunately, the IGLO II basis set for Sn does not appear to be in the public domain. Relativistic calculations using the zeroth order regular approximation with spin-orbit coupling (ZORA-SO) also give very good agreement with experimental results, even for Sn compounds with heavy atoms such as Br or I.³⁷

In this work, we apply the ZORA-SO method for ^{119}Sn chemical shift calculation to the conformer geometries optimized using the PBE0-GD3BJ level of theory. Using different levels of theory for geometrical optimization and chemical shift calculations is acceptable because the chemical shift is essentially a nuclear property influenced by electronic distributions rather than an intrinsically electronic property. Figure 5 shows the correlation between calculated and experimental ^{119}Sn chemical shifts for a series of non-hypercoordinate reference compounds with structural elements related to the methoxystannane substituents in this study and with a wide range of chemical shifts. The calculated geometries and ^{119}Sn NMR chemical shifts are for gas-phase molecules while the experimental chemical shifts were measured in a non-coordinating solvent (usually chloroform). A good linear agreement is obtained with a slope of 1.012, and a correlation coefficient of 0.9966. Because both experimental and calculated chemical shifts are relative to the chemical shift of SnMe_4 defined as 0 ppm, the regression must pass through the origin.

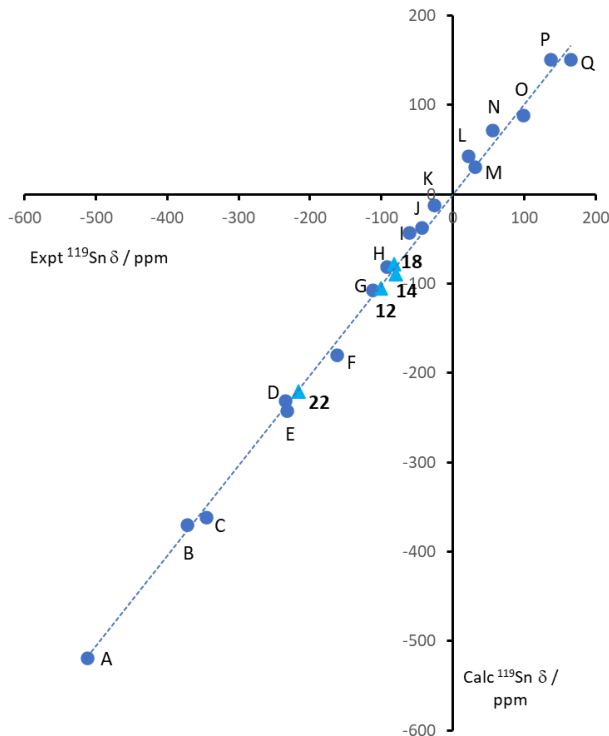


Figure 5. Correlation between calculated and experimental ^{119}Sn chemical shifts. The regression line is for non-hypercoordinate reference tin compounds A - Q (●): $\text{Calc } \delta = m (\text{Exp } \delta)$, $m = 1.012$, $r = 0.9966$. Chemical shifts for **12**, **14**, **18**, and **22** (▲) calculated for gas phase conformations with Boltzmann averaging using values in Tables S-2 and S-3 (see SI). Reference compounds: A: SnH_4 , B: $\text{Sn}(\text{CH}_3)_3$, C: PhSnH_3 , D: $\text{Sn}(\text{CH}_3)_2\text{H}_2$, E: Ph_2SnH_2 , F: Ph_3SnH , G: $\text{Sn}(\text{CH}_3)_3\text{H}$, H: Ph_3SnMe , I: PhSnCl_3 , J: Ph_3SnCl , K: Ph_2SnCl_2 , L: $\text{Sn}(\text{CH}_3)\text{Cl}_3$, M: $(p\text{-tBu-C}_6\text{H}_4)_2\text{Sn}(\text{CH}_3)\text{Cl}$, N: $\text{PhSn}(\text{CH}_3)\text{Cl}_2$, O: $\text{PhSn}(\text{CH}_3)_2\text{Cl}$, P: $\text{Sn}(\text{CH}_3)_2\text{Cl}_2$, Q: $\text{Sn}(\text{CH}_3)_3\text{Cl}$. Experimental ^{119}Sn chemical shifts: Ref. 43,44: A, B, D, G, L, O-Q; Ref. 40: C, E, F, I-K; Ref. 45: H; Ref. 46: M, N.

Using the same methodology, ^{119}Sn NMR chemical shifts were calculated for each of the methoxystannane conformers, as geometrically optimized in both gas and solvent phases (Table S-3). The calculated ^{119}Sn NMR chemical shifts are

sharply dependent on the Sn-O distances, with extended conformers having shifts close to non-hypercoordinate analogues but hypercoordinate conformers showing significant upfield shifts. Because the optimized geometries of the hypercoordinate conformers in solvent phase typically show shorter Sn-O distances, the calculated chemical shifts tend to be shifted more upfield than for the gas-phase geometries.

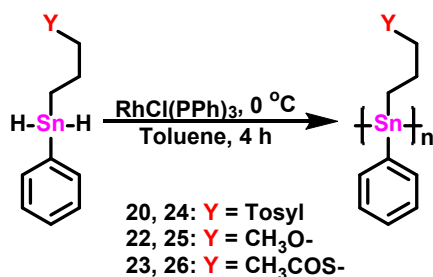
Using the estimated fractional abundances of the conformers (Table S-2) and the calculated chemical shifts (Table S-3), Boltzmann-averaged chemical shifts for compounds **12**, **14**, **18** and **22** were calculated (Figure 5, Table 1). Due to the relatively low Gibbs energy differences for the extended conformers of **12** and **22** in the solvent phase compared to the most stable hypercoordinate conformer, the corresponding calculated ^{119}Sn NMR chemical shifts are more approximate; higher energy non-hypercoordinate conformers would also need to be considered in the average. The Boltzmann averaged ^{119}Sn NMR chemical shifts for the gas phase geometries agree well with the experimental values, falling essentially on the linear correlation (Figure 5). The values for the compounds calculated with the chloroform solvent model are significantly lower.

On this basis, the PBE0-GD3BJ gas phase model appears to more accurately predict the conformer geometries/relative energies than the solution phase PCM: the condensed phase calculations seemingly overestimate the extent of hypercoordination and systematically underestimate the Sn-O distances. This points to a potential weakness in the “structural benchmarking” approach that has not been previously identified. The PBE0-GD3BJ method was originally selected on the basis of giving the best structural predictions for Sn hypercoordinate compounds in comparison with solid-state X-ray crystallographic structures. This approach may inadvertently factor in the effects of a condensed phase on relatively compressible interactions, such as the Sn-O hypercoordination, such that if the gas-phase calculation approximates it, a solution-phase calculation with the same functional will overestimate the strength and underestimate the distance. This suggests that alternative approach(s) are required for accurately modelling hypercoordinate interactions in solution.

Table 1. Experimental and Boltzmann-averaged calculated ^{119}Sn NMR chemical shifts for selected methoxystannanes

Compound	Expt ^{119}Sn δ /ppm	Calc ^{119}Sn δ /ppm (gas phase)	Calc ^{119}Sn δ /ppm (CHCl_3)
12	-101.4 ^a	-105.2	-109.9
14	-80.0 ^a	-89.7	-114.7
18	-82.1 ^a	-78.5	-103.8
22	-215.7 ^b	-220.3	-234.7

Dehydrocoupling Polymerizations



Scheme 3: Synthesis of methoxy, thioacetyl and tosyl homopolymers by dehydrocoupling polymerization.

The tosyl-containing polystannane **24**, as previously described, was prepared via a transition metal-catalyzed dehydrocoupling of **20** in a foil-wrapped Schlenk flask under a N_2 atmosphere (Scheme 3). These precautions are to (i) avoid the possibility of light degrading the monomer, (ii) suppress homolytic cleavage of the resulting polystannanes and (iii) prevent the formation of stannoxanes from nucleophilic attack by moisture, respectively. Polymer **24** was

purified by precipitation of a THF solution (3 mL) containing crude **24** into an excess of hexanes (100 mL) and thereafter recovered as an orange-coloured solid. GPC analysis in THF revealed a molecular weight (M_w) of 17 kDa and a \bar{D} of 1.26. The tosylated polymer **24** was also characterized by both ^1H and ^{119}Sn NMR (C_6D_6) spectroscopy and was in agreement with the reported literature values.¹⁷ A similar dehydrocoupling reaction of **22** was successfully carried out to yield polymer **25** which was recovered as a yellow coloured powder in moderate yields (64 %). A molecular weight determination of **25** after purification proved difficult as the polymer was almost completely insoluble in THF, the solvent required for analysis. Attempts to redissolve purified **25** in the original reaction solvent also proved futile, and all analyses were thus carried with crude **25** due to the apparent highly crystalline nature of the resulting polymer. NMR (^{119}Sn) analysis of the crude polystannane **25** prior to purification reveal evidence of partial hypercoordination with two nearly equally intense resonances at $\delta = -193$ and -238 ppm (Figure S53), similar to what was observed for the phenyl propyl hydroxyl stannane polystannane, **27** (Figure 5).¹⁷ These two signals represent both the “open” and “closed” configurations of the polymer where the methoxy group can potentially interact with a Sn centres.

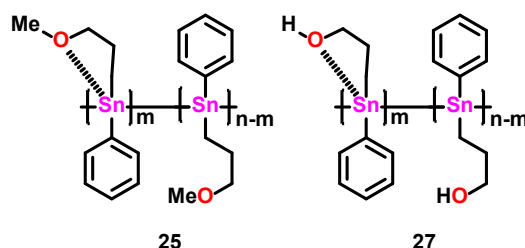


Figure 5: Open and closed conformations of stannanes centers in polymers **25** and **27**.

After a single purification, the polymer is notably less soluble and displays only a single ^{119}Sn resonance at -237.9 ppm (Figure S54), suggesting that the polymer likely migrates to a fully “closed” form. DSC analysis of homopolymer **25** reveals reversible semi-crystalline/highly crystalline character with $T_m = 127$ °C, and $T_g = 91$ °C (Figure S63), similar to that for **27** ($T_m = 110$ °C, and $T_g = 49$ °C) as previously reported.¹⁷ The PXRD diffractogram of **25** (Figure 6) shows five distinct signals. Two of the signals are intense and sharp in nature with 2θ values of 14.30° and 17.15° , while the remaining three signals are broad and less intense (2θ values of 6.35° , 18.93° and 25.90°). These values fall within the same range as other recently reported unsymmetrical polystannanes.^{15,17} The sharp signals in the PXRD diffractogram, in conjunction with the presence of a T_m in the DSC thermogram confirm that **25** is semi- to highly-crystalline in nature.

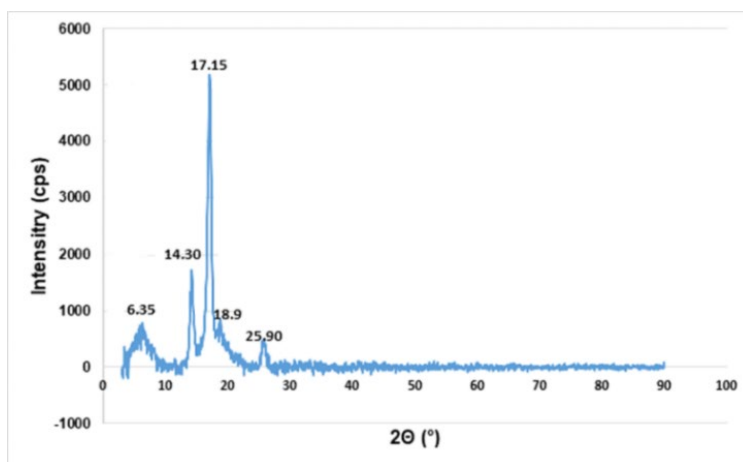
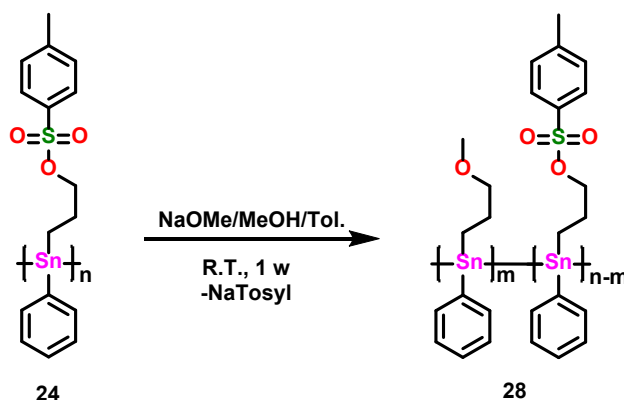


Figure 6: PXRD of homopolystannane **25** after purification.

Attempts to prepare the thioacetyl homopolymer **26** from **23** under similar protocols were unsuccessful owing largely to the extreme sensitivity of the polymer to light, which changed from a light yellow to a darker insoluble brown solid after a minimal exposure to light. Further explorations of this material were therefore abandoned.

Attempted Macromolecular substitution

Substitution of the tosyl substituent of **24** for a methoxy functionality was attempted (Scheme 4).



Scheme 4: Macromolecular substitution reaction to polystannane **28**.

After several attempts (Table S48), the optimized conditions for an S_N2 type substitution of **24** utilizing a 10:1 mixture of toluene and MeOH and one equivalent of NaOMe stirring at RT for 1 week were identified. The crude yellow coloured polymer, **28**, was gravity filtered to remove the resulting salts and the volatile components were then removed under reduced pressure. The substituted product, **28**, was further purified by redissolving the crude polymer in a minimum of THF and induced precipitation from this solution by adding it to an excess of cold hexanes. NMR spectroscopic analysis (¹H, ¹¹⁹Sn) of the substituted polymer suggests that **28** is ≈ 50% methoxy substituted. The ¹¹⁹Sn NMR (Figure S56) reveals chemical shift values typically of both the homopolymer **25** in open and closed conformations, as well as a resonance for the unsubstituted polymer **24**. A GPC analysis of the partially substituted polymer was not performed, as purified **28** was found to be insufficiently soluble in THF.

Conclusion

Nucleophilic substitution of a labile model tosylated triphenylstannane **4** to either aryloxy, alkoxy or thioacetate bearing stannanes in good yields was demonstrated. DFT optimization of individual molecules using the PBE0-GD3BJ method generally provided the best predictions of solid-state molecular properties. Modelling of hypercoordinate conformations for the methoxy- series **12**, **14**, **18**, and **22** with PBE0-GD3BJ showed that inclusion of the PCM solvent model predicts significantly shorter Sn-O distances than in the gas phase. Relativistic DFT calculations of ¹¹⁹Sn chemical shifts for these conformations with Boltzmann averaging closely approximated experimental values when gas phase geometries and conformer distributions were used but performed poorly with solvent phase ones. The selection of the PBE0-GD3BJ method by “structural benchmarking” gas-phase geometries to solid-state structures may have effectively factored in the impact of a condensed phase on the hypercoordinate interactions, causing the solvation model to overestimate these. A new light and moisture stable semicrystalline polystannane, **25**, was prepared by the dehydropolymerization in the presence of Wilkinson’s catalyst. Evidence for extensive hypercoordination was detected by ¹¹⁹Sn NMR spectroscopy. Access to the similar, but only partially substituted methoxy stannane, **28**, via an S_N2 reaction involving a tosylated polymeric intermediate **24** in good yields has also been demonstrated using mild reaction conditions. Despite the sensitivity of the Sn-Sn bonds of the labile polystannane, prolonged reaction periods (> 1 week) of tosyl containing polystannane **24** with a nucleophile in the absence of light can allow access to functionally stable new polystannanes.

Experimental

General remarks

¹H NMR (400 MHz), ¹³C NMR (100.6 MHz) and ¹¹⁹Sn NMR (149.2 MHz) spectra were recorded on a Bruker Advance 400 MHz NMR spectrometer with a BBFO 5-mm direct probe. A ¹H pulse width of 30° was used, acquiring a spectral window of 8223 Hz (20 ppm) using a relaxation delay of 1s, acquisition time 3.98s, 32k points (16 scans). The ¹H 90° pulse width

was 10.4 μ s. A ^{13}C pulse width of 30° was used, acquiring a spectral window of 24038 Hz (239 ppm) using a relaxation delay of 2s, acquisition time 1.36s, 32k points (4096 scans). The ^{13}C 90° pulse width was 8.7 μ s. A ^{119}Sn pulse width of 30° was used, 8.75 μ s, acquiring a spectral window of 100000 Hz (670 ppm) using a relaxation delay of 1s, acquisition time 0.33s, 32k points (15360 scans) with inverse gated proton decoupling. All results were analysed on MestReNova LITE 5.2.5 software. Chemical shifts were calculated using the chemical deuterated standards as a reference for ^1H and ^{13}C . The ^{119}Sn was referenced to SnMe_4 as an internal standard. All J coupling values are reported as absolute values. Time-of-flight mass spectrometry analyses were performed at the AIMS Mass Spectrometry Laboratory, University of Toronto using a JMS-T1000LC mass spectrometer (JEOL Inc., Peabody, MA) equipped with a Direct Analysis in Real Time (DART) ionization source (DART-SVP, Ionsense Inc., Saugus, MA). The DART source was operated with He gas and the temperature was adjusted in the range 100-400 $^\circ$ C. Isotopic distributions for the observed ionic species were calculated using the Mass Center utility (JEOL) and were in good agreement with the measured mass spectra. Absolute molecular weights of the polymers were determined by GPC using a Viscotek Triple Model 302 Detector system. GPC columns were calibrated versus polystyrene standards (American Polymer Standards). A flow rate of 1.0 mL/min. was used with ACS grade THF as the eluent. GPC samples were prepared using 3-10 mg of each polymer per mL THF, and filtered using a 0.45 μ m filter. All samples were run with and without UVA (conc. \approx 0.001 M) for comparison. The X-ray diffraction data for compounds **12**, **14**, **18**, and **19** were collected on a Bruker Kappa APEX-DUO diffractometer using monochromated Mo-K α radiation (Bruker Triumph) and were measured using a combination of θ scans and χ scans. The data were processed using APEX2 and SAINT programs. Absorption corrections were carried out using SADAB. The structures were solved using SHELXT⁴⁷ and refined using SHELXL-2013⁴⁷ for full-matrix least-squares refinement that was based on F^2 . For all structures, H atoms were included in calculated positions and allowed to refine in a riding-motion approximation with Uiso tied to the carrier atom. All reactions were carried out under a nitrogen atmosphere using Schlenk techniques unless otherwise described. LiAlH_4 (1.0 M in Et_2O), NaBH_4 , 1.0 M solution of HCl in Et_2O , anhydrous CaCl_2 , anhydrous MgCl_2 and Wilkinson's catalyst were purchased commercially and used without further purification. Solvents were dried by standard procedures prior to use.

3-(triphenylstannyl)propyl-4-methylbenzenesulfonate **4**

In a 250 mL round bottom flask, triphenyl(3-propylhydroxy)stannane (5.46 g, 13.4 mmol) and *p*-toluenesulfonyl chloride (3.83 g, 20.1 mmol) were dissolved in DCM (100 mL). Once dissolved, NEt_3 (3.73 mL, 26.8 mmol) was added, after which $\text{NMe}_3\cdot\text{HCl}$ (1.28 g, 13.4 mmol) was added to the solution. The mixture was allowed to react at RT for 2 h. The organic layer was washed with five aliquots of distilled water (DW, 50 mL), and the volatile components were removed under reduced pressure. The resulting gel was triturated with MeOH (3 \times 20 mL). The residual volatile components were removed under reduced pressure to yield the purified product as a white powder. Yield: 4.50 g, 60%. **Mp** = 76-77 $^\circ$ C. **$^1\text{H-NMR}$** (400 MHz, CDCl_3 , δ): 7.75 (d, $^3J_{1\text{H}-1\text{H}} = 12$ Hz, 2H, H4), 7.57-7.44 (m, $^3J_{117/119\text{Sn}-1\text{H}} = 48$ Hz, 6H, H10), 7.39-7.31 (m, 9H, H11 & H12), 7.30 (d, $^3J_{1\text{H}-1\text{H}} = 8$ Hz, 2H, H3), 4.02 (t, 2H, H6), 2.44 (s, 3H, H1), 2.10-1.94 (m, 2H, H7), 1.49-1.31 (m, 2H, H8) ppm; **$^{13}\text{C}\{^1\text{H}\}\text{-NMR}$** (100 MHz, CDCl_3 , δ): 144.94 (C5), 138.28 (C9), 137.28 (C10), 113.54 (C2) 130.13 (C4) 129.41 (C12), 128.95 (C11), 128.21 (C3), 73.34 (C6), 26.42 (C7), 21.96 (C1). 6.19. (C8) ppm; **$^{119}\text{Sn-NMR}$** (149 MHz, CDCl_3 , δ): -99.58 ppm. The NMR spectra obtained agreed with previously reported literature.¹⁵

(3-([1,1'-biphenyl]-4-yloxy)propyl)triphenylstannane **11**

Method A: In a 50 mL round bottom flask containing 25 mL of acetone was added compound **4** (0.50 g, 0.888 mmol), K_2CO_3 (0.16 g, 1.11 mmol) and 4-phenylphenol (0.15 g, 0.888 mmol). The reaction was heated (65 $^\circ$ C) to reflux with stirring for 72 h where a cloudy white solution was observed to form. Upon cooling, the acetone was removed *in vacuo* and redissolved with DCM (20 mL), filtered and washed with distilled H_2O (3 \times 20 mL). The organic phase was dried with MgSO_4 , filtered and brought to dryness on a rotovap. The crude product was washed with MeOH (3 \times 20 mL) to afford a white coloured powder of **11**. The NMR data was consistent with the previously reported literature.²⁶ Yield: 0.40 g (40%).

Method B. In a 100 mL round bottom flask, compound **4** (0.50 g, 0.89 mmol), K_2CO_3 (0.16 g, 1.11 mmol) and 4-phenylphenol (0.19 g, 1.11 mmol) were dissolved in ACN. The reaction was allowed to reflux for 72 h, after which the volatile components were removed under reduced pressure. The resulting product was redissolved in DCM and washed with 3 aliquots (50 mL) of a 5% aq. Na_2CO_3 solution. The organic phase was dried with anhydrous MgSO_4 and filtered, and the volatile components removed under vacuum to afford an off-white gel. The crude product was triturated with

MeOH (3 × 20 mL) to yield the pure product **11** as a white powder. Yield: 0.49 g, 98%. The NMR spectrum obtained agreed with previously reported data.²⁶

¹H-NMR (400 MHz, CDCl₃, δ): 7.63-7.54 (m, 6H, H13), 7.54-7.46 (m, 4H, H2 & H3), 7.44-7.40 (m, 2H, H6), 7.38-7.37 (m, 9H, H14 & H15), 7.32-7.29 (m, 1H, H1), 6.86-6.84 (d, ³J_{1H-1H} = 8 Hz, 2H, H7) 4.00 (t, 2H, H9), 2.24-2.23 (m, 2H, H10), 1.67-1.63 (m, 2H, H11) ppm. **¹¹⁹Sn{¹H}-NMR** (149 MHz, CDCl₃, δ): -99.42 ppm.

3-(methoxypropyl)triphenylstannane 12

In a 100 mL round bottom flask, **4** (0.50 g, 0.91 mmol) and 25% w/v NaOMe/MeOH (0.70 mL, 2.64 mmol) were combined and dissolved in 50 mL ACN. The solution was heated under reflux for 24 h, after which the ACN was removed under reduced pressure. The product was then redissolved in DCM and washed with aliquots (3 × 50 mL) of a 5% aq. Na₂CO₃ solution. The organic layer was dried with anhydrous MgSO₄, filtered, and the DCM removed under reduced pressure. The resulting solution was recrystallized in heptane to yield the purified product as white crystals. Yield: 0.34 g, 89%. **¹H-NMR** (400 MHz, CDCl₃, δ): 7.63-7.49 (m, ³J_{117/119Sn-1H} = 52 Hz, 6H, H6), 7.38-7.36 (m, 9H, H7 & H8), 3.38 (t, 2H, H2), 3.16 (s, 3H, H1), 2.04-1.97 (m, ³J_{117/119Sn-1H} = 64 Hz, 2H, H3), 1.55-1.51 (m, ²J_{117/119Sn-1H} = 56 Hz, 2H, H4) ppm; **¹³C{¹H}-NMR** (100 MHz, CDCl₃, δ): 139.40 (C5), 137.16 (C6), 128.87 (C8), 128.54 (C7), 75.37 (C2), 58.47 (C1), 26.61 (C3), 7.47 (C4) ppm; **¹¹⁹Sn{¹H}-NMR** (149 MHz, CDCl₃, δ): -100.00 ppm. HRMS: Calc: 443.0768, Found: 443.0729 m/z (M+Na)⁺.

(3-(triphenylstannyl)propyl) ethanethioate 13

In a 100 mL round bottom flask, **4** (4.79 g, 8.50 mmol), K₂CO₃ (1.47 g, 10.63 mmol) and thioacetic acid (0.60 mL, 8.50 mmol) were combined and dissolved in ACN. The mixture was allowed to stir at 26 °C for 48 h after which the solvent was removed under reduced pressure. The product was redissolved in DCM and washed with a 5% aq. Na₂CO₃ solution (3 × 75 mL). The DCM was dried using anhydrous MgSO₄ and filtered. The solvent was removed under reduced pressure affording the clean product **13**, as a light brown oil. Yield: 2.77 g, 70%. **¹H-NMR** (400 MHz, CDCl₃, δ): 7.67-7.54 (m, 6H, H7), 7.46-7.41 (m, 9H, H8 & H9), 2.99 (t, 2H, H3), 2.35 (s, 3H, H1), 2.11-1.94 (m, ³J_{117/119Sn-1H} = 76 Hz, 2H, H4), 1.70-1.52 (m, ²J_{117/119Sn-1H} = 76 Hz, 2H, H5) ppm; **¹³C{¹H}-NMR** (100 MHz, CDCl₃, δ): 194.58 (C2), 137.31 (C6), 135.93 (C7), 127.91 (C9), 127.50 (C8), 31.93 (C3), 29.57 (C1), 25.85 (C4), 8.96 (C5) ppm; **¹¹⁹Sn{¹H}-NMR** (149 MHz, CDCl₃, δ): -101.35 ppm. HRMS: Calc: 483.0488, Found: 485.0452 m/z (M+Na)⁺.

Chloro(3-methoxypropyl)diphenylstannane 14

In a 100 mL round bottom flask, **12** (0.32 g, 0.76 mmol) was dissolved in C₆H₆ (50 mL). An ethereal solution of 1.0 M HCl in Et₂O (0.76 mL, 0.76 mmol) was added to the stirring solution, and the mixture was allowed to react at RT for 1 h. The volatile components were removed under reduced pressure and the resulting product was recrystallized in heptane to yield the product as a white powder. Yield: 0.23 g, 80%. **¹H-NMR** (400 MHz, CDCl₃, δ): 7.78-7.63 (m, ³J_{117/119Sn-1H} = 52 Hz, 4H, H6), 7.45-7.36 (m, 6H, H7 & H8), 3.52 (t, 2H, H2), 2.95 (s, 3H, H1), 2.17-2.11 (m, ³J_{117/119Sn-1H} = 56 Hz, 2H, H3), 1.80-1.76 (m, ³J_{117/119Sn-1H} = 84 Hz, 2H, H4) ppm; **¹³C{¹H}-NMR** (100 MHz, CDCl₃, δ): 140.93 (C5), 136.18 (C6), 129.76 (C8), 128.98 (C7), 73.68 (C2), 58.87 (C1), 25.97 (C3), 15.28 (C4) ppm; **¹¹⁹Sn{¹H}-NMR** (149 MHz, CDCl₃, δ): -80.39 ppm. **HRMS-DART m/z**: [M+NH₄]⁺ Calculated 400.0483, Found 400.0481.

S-(3-(chloro(diphenylstannyl)propyl) ethanethioate 15

In a 100 mL round bottom flask, **13** (0.11 g, 0.24 mmol) was dissolved in C₆H₆ (50 mL). An ethereal solution of 1.0 M HCl in Et₂O (0.24 mL, 0.24 mmol) was added to the solution, and the mixture was allowed to react at RT for 1 h. The C₆H₆ was then removed under reduced pressure to afford a yellow-brown oil of **15**. Yield: 0.10 g, 99%. **¹H-NMR** (400 MHz, CDCl₃, δ): 7.77-7.46 (m, 4H, H7), 7.53-7.45 (m, 6H, H8 & H9), 2.97 (t, 2H, H3), 2.27 (s, 3H, H1), 2.19-2.12 (m, ³J_{117/119Sn-1H} = 68 Hz, 2H, H4), 1.91-1.72 ppm (m, ²J_{117/119Sn-1H} = 76 Hz, 2H, H5) ppm; **¹³C{¹H}-NMR** (100 MHz, CDCl₃, δ): 195.21 (C2), 137.82 (C6), 134.85 (C7), 129.12 (C9), 127.96 (C8), 31.06 (C3), 29.59 (C1), 24.82 (C4), 15.91 (C5) ppm; **¹¹⁹Sn{¹H}-NMR** (149 MHz, CDCl₃, δ): -0.98 ppm.

Dichloro(3-phenylstannyl)propyl) methylbenzenesulfonate 16

In a 100 mL round bottom flask, **4** (1.13 g, 2.01 mmol) was dissolved in C₆H₆ (50 mL). 1M HCl in Et₂O (2.01 mL, 2.01 mmol) was added to the stirring solution, and the mixture was allowed to react at RT. After 1h, 1M HCl in Et₂O (2.01 mL, 2.01 mmol) was added and the reaction was allowed to stir for an additional hour. The volatile components were removed under reduced pressure and the resulting product recrystallized in heptane to yield the purified product as a white powder. Yield: 0.93 g, 97%. The NMR spectrum obtained agreed with previously reported data.²² **¹H-NMR** (400

MHz, CDCl₃, δ): 7.73 (d, ³J_{1H-1H} = 8 Hz, 2H, H4), 7.66-7.64 (m, 2H, H10), 7.56-7.47 (m, 3H, H11 & H12), 7.33 (d, ³J_{1H-1H} = 8 Hz, 2H, H3), 4.14 (t, ³J_{1H-1H} = 6 Hz, 2H, H6), 2.44 (s, 3H, H1), 2.28-2.21 (m, ³J_{117/119Sn-1H} = 64 Hz, 2H, H7), 2.05-1.88 (m, ²J_{117/119Sn-1H} = 64 Hz, 2H, H8) ppm; ¹³C{¹H}-NMR (100 MHz, CDCl₃, δ): 145.50 (C5), 138.91 (C9), 135.15 (C10), 132.79 (C2), 131.92 (C12), 130.29 (C3), 129.86 (C11), 128.33 (C4), 71.37 (C6), 24.82 (C7), 22.00 (C1), 21.20 (C8) ppm; ¹¹⁹Sn-NMR (149 MHz, CDCl₃, δ): 30.79 ppm.

Dichloro(3-methoxypropyl)diphenylstannane 18

In a dry 50 mL Schlenk flask, compound **14** (0.10 g, 0.262 mmol) in C₆H₆ (30 mL) was added. Then an ethereal solution of 1.0 M HCl in Et₂O (1.76 mL, 1.28 g, 1.75 mmol) was added by syringe and stirred for 1 h at 0 °C. The residual solvent was removed *in vacuo* to obtain a white colored solid of **18** in near quantitative yield. Yield: 0.58 g (98 %). **Mp** = 99-100 °C. ¹H-NMR (400 MHz, CDCl₃, δ): 7.86-7.65 (m, ³J_{117/119Sn-1H} = 80 Hz, 2H, H6), 7.51-7.43 (m, 3H, H7 & H8), 3.62 (t, 2H, H2), 3.30 (s, 3H, H1), 2.22-2.17 (m, ³J_{117/119Sn-1H} = 24 Hz, 2H, H3), 2.10-1.85 (m, ²J_{117/119Sn-1H} = 88 Hz, 2H, H4) ppm; ¹³C{¹H}-NMR (100 MHz, CDCl₃, δ): 141.36 (C5), 135.30 (C6), 131.07 (C8), 129.49 (C7), 72.14 (C2), 59.00 (C1), 25.38 (C3), 22.59 (C4) ppm; ¹¹⁹Sn{¹H}-NMR (149 MHz, CDCl₃, δ): -83.53 ppm. **HRMS-DART m/z**: [M+NH₄]⁺ Calculated 357.9773, Found 357.9771.

S-(3-(dichloro(phenyl)stannyl)propyl) ethanethioate 19

In a 100 mL round bottom flask, **15** (0.10 g, 0.23 mmol) was dissolved in C₆H₆ (50 mL). An ethereal solution of 1M HCl in Et₂O (0.23 mL, 0.23 mmol) was added to the solution, and the mixture was allowed to react at RT for 1 h, after which the solvent was removed under reduced pressure to yield an on-off white powder. Yield: 0.080 g, 89%. **Mp** = 85°C. ¹H-NMR (400 MHz, CDCl₃, δ): 7.84-7.63 (m, 2H, H7), 7.54-7.43 (m, 3H, H8 & H9), 3.03 (t, 2H, H3), 2.27-2.20 (m, 2H, H4), 2.24 (s, 3H, H1), 2.08-1.90 (m, ²J_{117/119Sn-1H} = 64 Hz, 2H, H5) ppm; ¹³C{¹H}-NMR (100 MHz, CDCl₃, δ): 196.24 (C2), 139.95 (C6), 134.83 (C7), 131.35 (C8), 129.49 (C9), 31.35 (C3), 30.77 (C1), 25.10 (C4), 25.07 (C5) ppm; ¹¹⁹Sn{¹H}-NMR (149 MHz, CDCl₃, δ): 15.25 ppm. **HRMS-DART m/z**: [M+H₂O] Calculated 401.94927, Found 401.94892.

3-(phenylstannyl)propyl methylbenzenesulfonate 20

In a 100 mL Schlenk flask, **16** (0.50 g, 1.09 mmol) was dissolved in dry EtOH (12 mL) and allowed to stir on ice. In a 50mL Schlenk flask, NaBH₄ (0.35 g, 9.36 mmol) was dissolved in dry EtOH (6 mL) and allowed to stir on ice. The solution containing NaBH₄ was cannula transferred into the flask containing **16**. The mixture was allowed to react at 0 °C for 1 h, after which the reaction was quenched with degassed water. The product was extracted with hexane, which was then washed once with degassed water (25 mL). The organic layer was dried with anhydrous MgSO₄, filtered and the volatile components were removed under reduced pressure to yield the purified product as an off-white gel. Yield: 0.31 g, 69%. The NMR spectrum obtained agreed with previously reported data.²² ¹H-NMR (400 MHz, CDCl₃, δ): 7.74 (d, ³J_{1H-1H} = 8 Hz, 2H, H4), 7.37-7.22 (m, ³J_{117/119Sn-1H} = 52 Hz, 2H, H11) 7.13-7.11 (m, 3H, H9 & H10), 6.69 (d, ³J_{1H-1H} = 8 Hz, 2H, H3), 5.29 (s, ¹J_{117Sn-1H} = 1764 Hz, ¹J_{119Sn-1H} = 1820 Hz, 2H, H9), 3.70 (t, 2H, H6), 1.83 (s, 3H, H1), 1.56-1.34 (m, ³J_{117/119Sn-1H} = 88 Hz, 2H, H7), 0.79-0.61 (m, ³J_{117/119Sn-1H} = 60 Hz, 2H, H8) ppm; ¹¹⁹Sn-NMR (149 MHz, CDCl₃, δ): -215.26 ppm.

(3-methoxypropyl)(phenyl)stannane 22

In a 100 mL Schlenk flask, **18** (0.68 g, 1.78 mmol) was dissolved in Et₂O. A 1M LiAlH₄ in Et₂O (1.78 mL, 1.78 mmol) solution was added to the flask and placed on ice. The solution was allowed to react at 0 °C for 1 h, after which the reaction was quenched with degassed water. The organic layer was washed one with degassed water (50 mL) before being dried with anhydrous MgSO₄ and filtered. The organic component was removed under reduced pressure to yield the final product as a dull yellow gel. Yield: 0.40 g, 83%. ¹H-NMR (400 MHz, CDCl₃, δ): 7.57-7.43 (m, ³J_{117/119Sn-1H} = 52 Hz, 2H, H7), 7.19-7.13 (m, 3H, H8 & H9), 5.56 (s, ¹J_{117Sn-1H} = 1748 Hz, ¹J_{119Sn-1H} = 1828 Hz, 2H, H5), 3.08-3.05 (t, 2H, H2), 3.00 (s, 3H, H1), 1.85-1.61 (m, ²J_{117/119Sn-1H} = 84 Hz, 2H, H3), 1.15-0.97 (m, ³J_{117/119Sn-1H} = 56 Hz, 2H, H4) ppm; ¹³C{¹H}-NMR (100 MHz, C₆H₆, δ): 137.47 (C5), 137.36 (C6), 128.32 (C7), 128.24 (C8), 74.35 (C3), 57.56 (C2), 27.14 (C1), 5.51 (C4) ppm; ¹¹⁹Sn{¹H}-NMR (149 MHz, CDCl₃, δ): -215.64 ppm. **HRMS-DART m/z**: [M-H]⁺ Calculated 271.0139, Found 271.0144.

S-(3-(phenylstannyl)propyl) ethanethioate 23

In a 100 mL Schlenk flask, **19** (0.19 g, 0.49 mmol) was dissolved in dry EtOH (12 mL) and allowed to stir on ice. In a 50 mL Schlenk flask, NaBH₄ (0.17 g, 4.45 mmol) was dissolved in dry EtOH (6 mL) and allowed to stir on ice. The solution containing NaBH₄ was cannula transferred into the flask containing **19**. The mixture was allowed to react at 0 °C for 1 h, after which the reaction was quenched with degassed water. The product was extracted with hexane, which was then

washed once with degassed water (25 mL). The organic layer was dried with anhydrous MgSO_4 , filtered and the volatile components were removed under reduced pressure to yield the purified product, **23**, as an off-white gel. Yield: 0.09 g, 60%. $^1\text{H-NMR}$ (400 MHz, C_6D_6 , δ): 7.38-7.37 (m, 2H, H8), 7.13-7.12 (m, 3H, H9 & H10), 5.39 (s, $^1J_{117\text{Sn}-1\text{H}} = 1752 \text{ Hz}$, $^1J_{119\text{Sn}-1\text{H}} = 1832 \text{ Hz}$, 2H, H6), 2.70 (t, 2H, H3), 1.85 (s, 3H, H1), 1.69-1.61 (m, 2H, H4), 0.94-0.90 (m, 2H, H5) ppm; $^{13}\text{C}\{^1\text{H}\}\text{-NMR}$ (100 MHz, CDCl_3 , δ): 193.02 (C2), 136.56 (C8), 134.77 (C7), 127.82 (C9), 127.60 (C10), 31.49 (C3), 29.01 (C1), 27.23 (C4), 6.42 (C5) ppm; $^{119}\text{Sn}\{^1\text{H}\}\text{-NMR}$ (149 MHz, CDCl_3 , δ): -217.63 ppm. **HRMS-DART m/z** : $[\text{M-H}]^+$ Calculated 314.9860, Found 314.9862.

Synthesis of Substitutionally Labile Polystannane by Dehydrocoupling

Tosyl homopolystannane **24**

In a foil wrapped 100 mL Schlenk flask, a solution containing $\text{RhCl}(\text{PPh}_3)_3$ (0.027 g, 0.0291 mmol) in toluene (10 mL) and stirred at 0 °C for 15 min to activate the catalyst. Afterwards, **20** (0.30 g, 0.730 mmol) in toluene (10 mL) was added dropwise over 10 min to the catalyst solution and stirred at 0 °C for 4 h. The mixture was reduced in volume and dissolved again in dry THF. The solution was transferred dropwise to a 100 mL Schlenk flask containing a stirring solution of cold dry hexane (65 mL). A yellow orange precipitate was observed immediately and stirred for 5 min before settling. Solvent decanting was done using a Pasteur pipet, after which the residue of **24** was dried *in vacuo* to obtain a yellow orange solid. Yield: 0.20 g (67%). Mw = 17 kDa. $D = 1.26$.

Propylmethoxy Polystannane **25**

In a 100 mL Al foil wrapped Schlenk flask, Wilkinson's Catalyst (0.008 g, 0.008 mmol) was added and dissolved in toluene (30 mL). The mixture was allowed to stir on ice for 20 min. In a separate 100 mL Al foil wrapped Schlenk flask **22** (0.12 g, 0.44 mmol) was dissolved in toluene. The solution containing **22** was added to the stirring solution containing Wilkinson's Catalyst dropwise. The mixture was allowed to react at RT for 4 h, after which the toluene was removed under reduced pressure. The crude polymer **25** was redissolved in minimal THF (2 mL) and precipitated in a stirring solution of cold hexane (50 mL). The top layer of hexane was decanted, and the residual solvent removed under reduced pressure to yield **25** as a yellow-orange powder. Yield: 0.070 g, 64%.

$^1\text{H-NMR}$ (400 MHz, CDCl_3 , d): 7.77-7.45 (bm, 2H, H6), 7.07-6.98 (bm, 3H, H7 & H8), 3.17-2.93 (bm, 5H, H1 & H2), 1.76-1.23 (bm, 4H, H3 & H4) ppm; $^{13}\text{C}\{^1\text{H}\}\text{-NMR}$ (100 MHz, CDCl_3 , d): 134.60 (C5 & C6), 131.31 (C7), 130.40 (C8), 74.35 (C2), 56.72 (C1), 28.90 (C3), 24.45 (C4) ppm; $^{119}\text{Sn-NMR}$ (149 MHz, CDCl_3 , d): -237.90 ppm. E. A. Calc. C 44.66, H 5.25, Found. C 35.58, H 4.57.

Preparation of a Substituted MeO Polystannane **28**

In a 100 mL Al foil wrapped Schlenk flask, homopolymer **24** (0.45 g, 1.10 mmol) was added and dissolved in a 10:1 solution of toluene/MeOH (20 mL). Once dissolved, 25% w/v NaOMe/MeOH (0.23 mL, 1.06 mmol) was added to the solution. The mixture was allowed to stir at RT for 1 wk, after which the solution was filtered, and the volatile components removed. The crude polymer was dissolved in a minimal amount of THF (1-2 mL) and precipitated into a stirring solution of cold hexane (50 mL). The top layer of hexane was decanted, and the residual solvent was removed under reduced pressure to afford **28** as an off-white powder. Yield: 0.170 g, 57%.

$^1\text{H-NMR}$ (400 MHz, C_6D_6 , d): 7.82-7.62 (bm, 2H, H6), 7.25-7.18 (bm, 2H, H7), 6.85-6.77 (bm, 1H, H8), 3.26-2.78 (bm, 3H, H1), 2.10-1.16 (bm, 6H, H2, H3 & H4); $^{119}\text{Sn-NMR}$ (149 MHz, C_6D_6 , d): -203.05, -236.67 ppm.

Computational Details

The Gaussian 16 suite of programs was used for all geometric optimizations and frequency calculations (G16 Rev C.01). $^{\text{48}}$ DFT was implemented with four density functionals (PBE0 "PBE1PBE", M05-2X, B3-PW91, and MN15) supplemented with Grimme's D3 empirical dispersion function and, with the exception of M05-2X, Becke-Johnson damping. $^{\text{30}}$ The LANL08d basis set (obtained from the Basis Set Exchange) $^{\text{49}}$ was used for Sn, and the 6-31+G(d,p) basis set for all other atoms, as a reasonable compromise between accuracy and computational cost. $^{\text{50, 51}}$ Tight convergence criteria and superfine integration grids were used for all geometry optimizations, in each case with verification by frequency calculation that a potential energy minimum had been located. Counterpoise corrections in calculations of dimers were applied during geometrical optimizations and frequency calculations. Cartesian coordinates for experimental structures were extracted from crystallographic information files (.cif) with OpenBabelGUI. $^{\text{52}}$ Solvation was implemented with the default Gaussian 16 method (the Polarizable Continuum Model using the integral equation formalism variant (IEF-

PCM).⁵³ Conformer fractions for compounds were calculated by determining $q_i = \alpha e^{-\Delta G/RT}$ for each conformer i , where α is the total degeneracy of the conformer. Dividing q_i by the sum of all q gives the fraction of conformer i . The Amsterdam density functional code (ADF/2017.207)⁵⁴ was used to calculate single point energies by the relativistic zeroth-order regular approximation (ZORA) method with optimized TZP basis sets and the PBE0 method with 50% Hartree-Fock exchange. ¹¹⁹Sn chemical shifts were determined with the ADF nmr property module⁵⁵ at the PBE0-50/TZP spin-orbit level. SnMe₄ (geometrically optimized as above) was used as the reference to determine relative chemical shifts. Boltzmann-averaged ¹¹⁹Sn chemical shifts were determined by summing the product of the chemical shift and the conformer fraction for each conformer.

Conflicts of interest

“There are no conflicts to declare”.

Acknowledgements

This work was supported by the NSERC Discovery Grant program. Computational studies (Wylie, Silverthorne) were made possible by the facilities of Compute/Calcul Canada and the Ryerson Analytical Facility.

Supplementary Material

Crystallographic Data was deposited with the following CCDC numbers (#2102113 **12**, #2102119 **14**, #2102115 **18**, and #2102113 **19**).

References

- 1 A.G. Davies, *Organotin Chemistry*, Wiley-VCH, Weinheim, 2nd edn., 2004.
- 2 A. U. Khan and D. A. Foucher, in *Main Group Strategies towards Functional Hybrid Materials*, eds. T. Baumgartner and F. Jäkle, John Wiley & Sons, Inc., 2017, pp. 209–236.
- 3 N. Devylder, M. Hill, K. C. Molloy and G. J. Price, *J. Chem. Soc., Chem. Commun.*, 1996, 711–712.
- 4 P. R. Deacon, N. Devylder, M. S. Hill, M. F. Mahon, K. C. Molloy and G. J. Price, *J. Organomet. Chem.*, 2003, **687**, 46–56.
- 5 D. Miles, T. Burrow, A. Lough and D. Foucher, *J. Inorg. Organomet. Polym. Mater.*, 2010, **20**, 544–553.
- 6 M. Okano, N. Matsumoto, M. Arakawa, T. Tsuruta and H. Hamano, *Chem. Commun.*, 1998, 1799–1800.
- 7 M. Okano and K. Watanabe, *Electrochem. Commun.*, 2000, **2**, 471–474.
- 8 T. Imori and T. D. Tilley, *J. Chem. Soc. Chem. Commun.*, 1993, 1607–1609.
- 9 V. Lu and T. D. Tilley, *Macromolecules*, 1996, **29**, 5763–5764.
- 10 V. Y. Lu and T. D. Tilley, *Macromolecules*, 2000, **33**, 2403–2412.
- 11 J. T. B. H. Jastrzebski and G. Van Koten, *Adv. Organomet. Chem.*, 1993, **35**, 241–294.
- 12 A. Růžička, R. Jambor, J. Brus, I. Císařová and J. Holeček, *Inorganica Chim. Acta*, 2001, **323**, 163–170.
- 13 I. A. Portnyagin, V. V. Lunin and M. S. Nechaev, *J. Organomet. Chem.*, 2008, **693**, 3847–3850.
- 14 S. Touqeer, L. Castoldi, T. Langer, W. Holzer and V. Pace, *Chem. Commun.*, 2018, **54**, 10112–10115.
- 15 J. Pau, A. J. Lough, R. S. Wylie, R. A. Gossage and D. A. Foucher, *Chem. Eur. J.*, 2017, **57**, 14367–14374.
- 16 K. A. Günay, P. Theato and H.-A. Klok, in *Functional Polymers by Post-Polymerization Modification: Concepts, Guidelines, and Applications*, eds. P. Theato and H. Klok, Wiley-VCH, 2013, pp. 1–44.
- 17 J. Pau, G. M. D’Amaral, A. J. Lough, R. S. Wylie and D. A. Foucher, *Chem. Eur. J.*, 2018, **24**, 18762–18771.
- 18 M. Mantina, A. C. Chamberlin, R. Valero, C. J. Cramer and D. G. Truhlar, *J. Phys. Chem. A*, 2009, **113**, 5806–5812.
- 19 T. Munguia, M. Lo, F. Cervantes-lee, K. H. Pannell, V. Uni and E. Paso, *Inorg. Chem.*, 2007, **46**, 1305–1314.
- 20 A. Khan, S. Komejan, A. Patel, C. Lombardi, A. J. Lough and D. A. Foucher, *J. Organomet. Chem.*, 2015, **776**, 180–191.
- 21 T. Lebl, A. Smicka, J. Brus and C. Bruhn, *Eur. J. Inorg. Chem.*, 2003, 143–148.
- 22 A. W. Addison, T. N. Rao, J. Reedijk, J. van Rijn and G. C. Verschoor, *J. Chem. Soc., Dalton. Trans.*, 1984, 1349–1356.
- 23 A. Khan, J. Pau, J. Loungxay, T. Magobenny, R. S. Wylie, A. J. Lough and D. Foucher, *J. Organomet. Chem.*, 2019, **900**, 120910.
- 24 D. N. Bender, A. J. Lough, R. S. Wylie, R. A. Gossage and D. A. Foucher, *Inorganics*, 2020, **8**, 1–22.
- 25 S. L. Hinchley, D. A. Wann and D. W. H. Rankin, *Int. J. Quantum Chem.*, 2005, **101**, 878–884.
- 26 P. D. McCaffrey, R. J. Mawhorter, A. R. Turner, P. T. Brain and D. W. H. Rankin, *J. Phys. Chem. A*, 2007, **111**, 6103–6114.
- 27 S. F. Sousa, E. S. Carvalho, D. M. Ferreira, I. S. Tavares, P. A. Fernandes, M. J. Ramos and J. A. N. F. Gomes, *J. Comput.*

- Chem.*, 2009, **30**, 2752–2763.
- 28 J. P. Perdew, in *Electronic Structure of Solids '91*, eds. P. Ziesche and H. Eschig, Akademie Verlag, Berlin, Germany, 1991, pp. 11–20.
- 29 J. P. Perdew, K. Burke and M. Ernzerhof, *Phys. Rev. Lett.*, 1996, **77**, 3865–3868.
- 30 S. Grimme, S. Ehrlich and L. Goerigk, *J. Comput. Chem.*, 2011, **32**, 1456–1465.
- 31 Y. Zhao, N. E. Schultz and D. G. Truhlar, *J. Chem. Theory Comput.*, 2006, **2**, 364–382.
- 32 H. S. Yu, X. He, S. L. Li and D. G. Truhlar, *Chem. Sci.*, 2016, **7**, 5032–5051.
- 33 H. S. Yu, X. He, S. L. Li and D. G. Truhlar, *Chem. Sci.*, 2016, **7**, 6278–6279.
- 34 Y. Izato, A. Matsugi, M. Koshi and A. Miyake, *Phys. Chem. Chem. Phys.*, 2019, **21**, 18920–18929.
- 35 L. B. Krivdin, *Russ. Chem. Rev.*, 2021, **90**, 1166–1212.
- 36 R. Vivas-Reyes, F. De Proft, M. Biesemans, R. Willem and P. Geerlings, *J. Phys. Chem. A*, 2002, **106**, 2753–2759.
- 37 A. Bagno, G. Casella and G. Saielli, *J. Chem. Theory Comput.*, 2006, **2**, 37–46.
- 38 P. Matczak, *MAIN Gr. Met. Chem.*, 2008, **31**, 189–202.
- 39 P. Matczak, *MAIN Gr. Met. Chem.*, 2009, **32**, 309–320.
- 40 C. Zeppek, J. Pichler, A. Torvisco, M. Flock and F. Uhlig, *J. Organomet. Chem.*, 2013, **740**, 41–49.
- 41 L. Broeckeaert, J. Turek, R. Olejnik, A. Ruzicka, M. Biesemans, P. Geerlings, R. Willem and F. De Proft, *Organometallics*, 2013, **32**, 2121–2134.
- 42 K. K. Pandey, *J. Organomet. Chem.*, 2016, **815–816**, 23–34.
- 43 B. Wrackmeyer, *Annu. Reports NMR Spectrosc.*, 1985, **16**, 73–186.
- 44 B. Wrackmeyer, *Annu. Reports NMR Spectrosc.*, 1999, **38**, 203–264.
- 45 M. Saito, Y. Okamoto and M. Yoshioka, *Appl. Organomet. Chem.*, 2005, **19**, 894–897.
- 46 R. N. Kapoor, P. Apodaca, M. Montes, F. D. Gomez and K. H. Pannell, *Appl. Organomet. Chem.*, 2005, **19**, 518–522.
- 47 G. M. Sheldrick, *Acta Cryst.*, 2015, **C71**, 3–8.
- 48 M. J. Frisch, G. W. Trucks, H. B. Schlegel, G. E. Scuseria, M. A. Robb, J. R. Cheeseman, G. Scalmani, V. Barone, G. A. Petersson, H. Nakatsuji, X. Li, M. Caricato, A. V. Marenich, J. Bloino, B. G. Janesko, R. Gomperts, B. Mennucci, H. P. Hratchian, J. V. Ortiz, A. F. Izmaylov, J. L. Sonnenberg, D. Williams-Young, F. Ding, F. Lipparini, F. Egidi, J. Goings, B. Peng, A. Petrone, T. Henderson, D. Ranasinghe, V. G. Zakrzewski, J. Gao, N. Rega, G. Zheng, W. Liang, M. Hada, M. Ehara, K. Toyota, R. Fukuda, J. Hasegawa, M. Ishida, T. Nakajima, Y. Honda, O. Kitao, H. Nakai, T. Vreven, K. Throssell, J. A. Montgomery, Jr., J. E. Peralta, F. Ogliaro, M. J. Bearpark, J. J. Heyd, E. N. Brothers, K. N. Kudin, V. N. Staroverov, T. A. Keith, R. Kobayashi, J. Normand, K. Raghavachari, A. P. Rendell, J. C. Burant, S. S. Iyengar, J. Tomasi, M. Cossi, J. M. Millam, M. Klene, C. Adamo, R. Cammi, J. W. Ochterski, R. L. Martin, K. Morokuma, O. Farkas, J. B. Foresman and D. J. Fox, *Gaussian 16, Rev. C. 01*, 2016.
- 49 B. P. Pritchard, D. Altarawy, B. Didier, T. D. Gibson and T. L. Windus, *J. Chem. Inf. Model.*, 2019, **59**, 4814–4820.
- 50 S. R. Whittleton, R. J. Boyd and T. B. Grindley, *J. Phys. Chem. A*, 2006, **110**, 5893–5896.
- 51 P. Matczak, *Comput. Theor. Chem.*, 2012, **983**, 25–30.
- 52 N. M. O'Boyle, M. Banck, C. A. James, C. Morley, T. Vandermeersch and G. R. Hutchison, *J. Cheminform.*, DOI:10.1186/1758-2946-3-33.
- 53 J. Tomasi, B. Mennucci and R. Cammi, *Chem. Rev.*, 2005, **105**, 2999–3093.
- 54 G. te Velde, F. M. Bickelhaupt, E. J. Baerends, C. F. Guerra, S. J. A. Van Gisbergen, J. G. Snijders and T. Ziegler, *J. Comput. Chem.*, 2001, **22**, 931–967.
- 55 G. Schreckenbach and T. Ziegler, *J. Phys. Chem.*, 1995, **99**, 606–611.